

Chapter 1

Overview

“When making an axe handle, the pattern is near at hand.”

– Lu Ji


Scientific discovery is driven by observations. Before 2015, **all** such observations and corresponding scientific conclusions were founded on the detection of **photons**, the messenger of the electromagnetic (EM) interaction.^a At 09:50 UTC on September 14, 2015 the laser interferometer gravitational wave observatory (LIGO) observed the universe for the first time in gravitons, or **gravity** waves (GWs), the messenger of the gravitational interaction ([Abbott et al. 2016b](#)). Even before the detection of GWs, the importance of combining information from EM and gravitational views was recognized (*e.g.* [Thorne & Braginskii 1976](#); [Phinney 2009](#)). The work laid out in this thesis is a contribution to this effort, to **maximize our observations** of GW sources by predicting the nature of EM signatures that should accompany them, or signify their existence beforehand. Such an endeavor not only provides ways to find sources of GWs and learn about their operation, but also drives investigation into the astrophysics that creates GW sources, and into the workings of



^aplus a few neutrinos ([Haxton et al. 2013](#); [Hirata et al. 1987](#); [Bionta et al. 1987](#); [IceCube Collaboration 2013](#))

physical processes in the extreme environments that generate gravitational radiation. We proceed by briefly discussing the expected sources of GWs, their detection, and the utility of their possible EM signatures. We then introduce two specific GW sources that are the topic of this thesis.

1.0.1 The gravitational side

Gravitational radiation is generated by the **acceleration** of **quadrupole** or higher moments of a mass-energy distribution. The result is the generation of metric perturbations 

$$h_{ij} = \frac{2G}{dc^4} \ddot{Q}_{ij}, \quad (1.1)$$

that propagate through spacetime as gravitational waves, carrying the information of a changing gravitational field (Wald 1984, *e.g.*). Here G and c are the usual gravitational constant and the speed of light, while d is the distance from observer to source of radiation, \ddot{Q}_{ij} is the second time derivative of the mass-energy quadrupole tensor and h_{ij} is the dimensionless strain tensor which measures fractional changes in proper distances. The units of \ddot{Q}_{ij} are a mass times a velocity squared. Hence you can **envision** the wave amplitude as being set by twice the kinetic energy put into **accelerating** the **quadrupolar** moment of a mass-energy distribution, times a coupling constant $2Gc^{-4}d^{-1}$. The coupling constant is determined by the strength of the **quadrupolar** tidal field; the minuscule size of this coupling constant is perhaps the reason why it has taken a century since their prediction to detect gravitational waves. For example, the gravitational wave strain from two point masses of total mass M , on a circular orbit of separation a is of order

$$h \sim \frac{2G}{dc^4} Mv^2 \sim \frac{GM}{ac^2} \frac{GM}{dc^2}. \quad (1.2)$$

Even for a binary consisting of two suns, orbiting as rapidly as possible, $a = R_\odot$, and within our galaxy $d \sim 1$ kpc the strain is incredibly small: $h \sim 10^{-22}$.

To experience gravitational wave strains of order unity, one must put a detector at a distance $d = 2GMc^{-2}(v/c)^2$ from a system of mass M and with typical velocities v . This distance is of order the gravitational radius, or the event horizon scale of a black hole. As we have not yet built black holes in a laboratory, we look to astrophysical sources. The best known astrophysical sources that approach these dimensions, and could occur close enough and frequently enough to be detectable, are the mergers of two (or more) compact objects, namely black holes (BHs), neutron stars (NSs), and white dwarfs (WDs) (*e.g.* [Thorne & Braginskii 1976](#); [Clark & Eardley 1977](#); [Belczynski et al. 2016](#)), cosmic inflation ([Starobinskiĭ 1979](#)) or (*e.g.* [Chiara Guzzetti et al. 2016](#), for a recent review), cosmological defects such as cosmic strings (*e.g.* [Damour & Vilenkin 2005](#), and references therein), non-axisymmetric features of rapidly spinning Neutron stars (*e.g.* [Haskell et al. 2015](#), and references therein), and core-collapse supernovae (*e.g.* [Fryer & New 2011](#), and references therein). For the remainder of this thesis we focus on the first example, and specifically the mergers BHs and NSs binaries.

There are multiple methods for detecting gravitational waves from merging compact objects. Just as for EM radiation, detector design depends on the radiation frequency. The gravitational wave frequency for a binary on a circular orbit is given by twice the orbital frequency^b

$$f_{\text{GW}} = 2f_{\text{orb}} \approx \frac{1}{\pi} \sqrt{\frac{GM}{a^3}} = \frac{1}{\pi} t_G^{-1} \left(\frac{a}{r_G} \right)^{-3/2} \quad (1.3)$$

where M is the total binary mass and a is the binary separation and $t_G \equiv GMc^{-3}$ is the gravitational time while $r_G \equiv GMc^{-2}$ is the gravitational radius. For astrophysical black holes, which range in mass from $\sim 1M_\odot \rightarrow 10^{10}M_\odot$, the gravitational wave frequency covers ten orders of

^bEccentric orbits emit gravitational waves over a spectrum of frequencies spanning the circular frequency and its higher order harmonics (*e.g.* [Enoki & Nagashima 2007](#)).

magnitude. Assuming $a = 2GM/c^2$ at merger, this range gives $f_{\text{GW}} = 10^4 \rightarrow 10^{-6}$ Hz. Considering also GW emission during the inspiral stage, the largest black holes emit at frequencies of $f_{\text{GW}} \sim 10^{-9}$ Hz at separations of order $100GM/c^2$.

This wide range of astrophysically interesting frequencies is currently covered by three different detector designs. From high to low frequencies, the first two use laser interferometers to detect the very small distance change between two test masses when a GW passes through them. The laser interferometer gravitational wave observatory (LIGO) is sensitive to GW frequencies ranging from $\sim 10 \rightarrow 10^4$ Hz with a peak strain sensitivity at $\sim 10^2$ Hz of $h \gtrsim 10^{-22}$ (LIGO Scientific Collaboration et al. 2015). This makes LIGO sensitive to the inspiral, merger, and ringdown of stellar mass compact object binaries consisting of BHs and NSs. LIGO could also detect GWs from the mountains on millisecond pulsars (*e.g.* Aasi et al. 2016, and references therein), or the stellar oscillations due to giant core collapse supernovae (*e.g.* Abbott et al. 2016a, and references therein). LIGO's localization capabilities are limited to a rather broad **~few square degrees**, but will increase when the two existing interferometers are joined by their international counterparts: VIRGO (Acernese et al. 2015) in Italy, GEO600 in Germany (Dooley & LIGO Scientific Collaboration 2015), KAGRA being built in Japan (Tomaru 2016), and in LIGO-India approved in March of 2016 (LIGO-India 2015).

At frequencies below ~ 1 Hz, **earth related vibrations** swamp the LIGO sensitivity making detection of sub Hz sources impossible (LIGO Scientific Collaboration et al. 2015). For this reason, space based interferometers were envisioned (Thorne & Braginskii 1976). Presently, the leading design is embodied in the eLISA mission, planned to be sensitive to GWs with frequency in the range $10^{-5} \rightarrow 1$ Hz with a peak sensitivity of $h \gtrsim 10^{-23}$, over a range of $0.01 \rightarrow 0.1$ Hz (Amaro-Seoane et al. 2013). eLISA will be oriented in a orbit around the Sun such that its changing orientation in time will allow localization of sources to within a **square degree** (Amaro-Seoane et al. 2013). LISA sources include the inspiral and merger of $10^4 \rightarrow 10^7 M_{\odot}/(1+z)$ MBHBs

in galactic nuclei at redshift z , the orbits of thousands of galactic binaries, extreme mass ratio inspirals of compact objects, stochastic GWs from the early universe ([Amaro-Seoane et al. 2013](#)), and the inspiral of NS and stellar BH binaries before they reach the LIGO band (*e.g.* [Sesana 2016](#), and references therein).

A second type of gravitational wave detector looks to nature’s clocks, the pulsars, to act as a galactic timing array. The so-called Pulsar Timing Arrays (PTAs) search for deviations in the arrival time of the pulses from millisecond pulsars. Timing deviations on the order of nano-seconds, correlated over multiple pulsars in our galaxy would signify the presence of very long wavelength gravitational waves, with frequencies ranging from $\sim 10^{-9} \rightarrow 10^{-6}$ Hz (wavelengths of parsecs to mill- parsecs!). Such low frequency radiation is expected from the inspiral of the largest BHs in the universe in galactic centers. For the closest ($z \lesssim 1$) MBHB inspirals, the PTAs could pick out the GW signal from an individual event, otherwise the PTAs will measure a stochastic background of GWs from MBHBs spiraling together throughout the universe. The magnitude and frequency dependence of the GW background holds information on the role of gas and stars in driving the binary inspiral through the PTA band and is an important probe of the MBHB population (*e.g.* [Sesana 2015](#)). The PTAs may also be sensitive to more exotic sources of gravitational radiation including the interactions of cosmic strings. Localization of individual GW sources by the PTAs will be constrained to a few to tens of square degrees ([Ellis et al. 2012](#)). Currently there are three active groups monitoring pulsars for use as a GW detector, the Parkes Pulsar Timing Array (PPTA [Hobbs 2013](#)), the European Pulsar Timing Array (EPTA [Kramer & Champion 2013](#)), and the North American Nanohertz Observatory for Gravitational Waves (NANOGrav [McLaughlin 2013](#)). The International Pulsar Timing Array (IPTA [Hobbs et al. 2010](#); [Manchester & IPTA 2013](#)) is a consortium between these groups.

1.0.2 The electromagnetic side

When black holes interact with gas and strong electromagnetic fields, they are sources of bright EM radiation on their own (*e.g.* active galactic nuclei and x-ray binaries). Boasting surface fields of $\sim 10^{12}$ G and up, neutron stars carry with them an enormous supply of potential EM energy and are themselves observable within our Galaxy. It is thus plausible that, in pairs, BHs and NSs could generate bright EM emission. Due to the potential modulation of an EM signal from binary orbital motion, as well as extreme energies that can be experienced at the end of the binary death spiral, such a signature may not only be bright, but uniquely identifiable as well. The benefit of EM signatures to GW events has been examined extensively in the literature (*e.g.* [Bloom et al. 2009](#)), here we survey some of the key points.

If an electromagnetic signature can be identified with a GW event, we call it an EM counterpart. Such an EM counterpart will allow localization of the GW source on the sky, which as we saw above, is not easy to do with GWs alone. Locating a bird by listening to its song vs. sighting it with your eyes, comes close to the analogous problem of identifying a source location with multiple gravitational wave detectors vs. pin-pointing its location with a telescope. For LISA-like detectors, sky localization improves the precision of the distance measurement, as this is largely limited by pointing error ([Cutler 1998](#); [Hughes 2002](#)). Localization will also give us contextual clues to the nature of the source, constraining formation scenarios.

If an EM observation yields not just a sky localization but also a redshift, the corroboration of a GW measured distance and an electromagnetically measured redshift can yield a precise measurement of the Hubble constant and other cosmological parameters ([Schutz 1986](#); [Krolak & Schutz 1987](#); [Chernoff & Finn 1993](#); [Schutz 2002](#); [Holz & Hughes 2005](#); [Dalal et al. 2006](#); [Kocsis et al. 2006](#); [Kocsis et al. 2008](#); [Cutler & Holz 2009](#); [Nissanke et al. 2010](#); [Nishizawa et al. 2011](#); [Taylor & Gair 2012](#); [Tamanini et al. 2016](#)) as well as constrain fundamental physics such as the nature of



gravity on large scales (Deffayet & Menou 2007; Camera & Nishizawa 2013).

EM counterparts can make independent measurements of binary parameters, removing degeneracies in their determination (Hughes & Holz 2003), and they can be used to reduce the signal to noise for GW detection (Kochanek & Piran 1993; Harry & Fairhurst 2011). In general, EM counterparts are vital to determining the astrophysical context of gravitational wave sources, allowing independent GW and EM measurements to constrain models for EM emission (Phinney 2009; Mandel & O’Shaughnessy 2010). The models for EM emission from BHNS mergers (Part II) could soon be vetted in this way with LIGO observations.

EM signatures are useful even when they cannot be GW counterparts. There are two types of EM signatures that are not counterparts. The first is purely a practicality: an EM signature that would be a counterpart, but cannot be not due to the source being out of the detectable distance or frequency range of a detector (or in the extreme limit, the detector does not yet exist). These EM signatures are useful in that they probe a missing part of the population of sources and provide proof of existence in the case of unbuilt instruments - if a tree falls in the woods, we could still see it! An example is gamma ray bursts (GRBs) that occur today outside of the LIGO volume or any inspiraling MBHBs which occur this decade in the LISA band. These are of course potential EM counterparts; given time and technology all such sources are EM counterparts. ^c

The second type of EM signature has no detectable GW counterpart by design. But rather these fundamentally lonely EM signatures survey a part of a GW source evolution before or after GW emission. For example, the early inspiral of MBHBs (e.g. Haiman et al. 2008, 2009) or the consequences of a BH kick after merger (e.g. Rosotti et al. 2012). Each of these EM signatures can allow us a glimpse into the broader evolution of the binary system. The primary focus of Part I of this thesis is to make predictions for the nature of EM signatures from the stage of MBHB evolution where the two black holes are interacting with a gas disk. As we discuss in the next

^cas long as they occur after the surface of last scattering for photons – the cosmic microwave background!

section, this stage can overlap with a regime where the binary is emitting GWs detectable by the PTAs and LISA, but the portion of inspiral before the binary is in any GW band can provide unique EM identifiers of the binary which can teach us about the environment of the central nucleus, the ‘final parsec problem’, and in general the MBHB path to coalescence.

The specific sources of GWs studied in this thesis are the inspiral and merger of MBHBs in galactic nuclei and the merger of magnetized NSs with $\gtrsim 10M_{\odot}$ BHs. I now give background on each source in turn.

1.1 Part I: Massive Black Hole Binaries

1.1.1 Formation of MBHBs

The discovery of stellar mass BHs was textbook. In the 1970’s X-ray astronomy pioneers Ricardo Giacconi and Herbert Friedman lead groups that carried out targeted searches for objects which consist of a strong X-ray source orbiting a strong optical source, the X-ray source thought to be emission from a BH accretion disk, fed by the optical source, a star. Such systems **were** envisioned from the theories of BH accretion and stellar evolution. These predictions were confirmed observationally and called the X-ray binaries, the first evidence of astrophysical BHs (an entertaining historical account is found in [Thorne 1994](#)).

The discovery of black holes millions to billions of times the mass of the Sun, however, came as a great surprise. It was not predicted that the enigma of the Quasars (*e.g.* [Schmidt 1963](#); [Salpeter 1964](#); [Lynden-Bell 1969](#)) would lead to our present day understanding that a massive black hole (MBH) of $10^5 \rightarrow 10^{10}M_{\odot}$ resides at the heart of nearly every galaxy ([Kormendy & Richstone 1995](#); [Kormendy & Ho 2013](#); [Ferrarese & Ford 2005](#)).

Further insight from cosmology adds to the story of MBHBs. The hierarchical formation of large scale structure, which is now standard lore of the Λ CDM cosmology, suggests that these MBH

harboring galaxies merge (Haehnelt & Kauffmann 2002). Indeed we see direct evidence of this in images of such mergers taking place on the $\gtrsim 100$ kpc scale (Comerford et al. 2013), (see also Dotti et al. 2012, and references therein), as well as dual active galactic nuclei (AGN) at the $\lesssim 1$ kpc scale (Komossa 2003; Fabbiano et al. 2011; Rodriguez et al. 2006; Burke-Spolaor 2011; Colpi & Dotti 2011; Gitti et al. 2013; Woo et al. 2014; Andrade-Santos et al. 2016)

Based on the observations that galaxy centers harbor MBHs and galaxies merge, the seminal paper by Begelman et al. (1980) first proposed that some galactic nuclei may harbor two MBHs, and that these may **form into** a massive black hole binary (MBHB) which could eventually merge via emission of gravitational radiation.

In this picture, the mass of the black hole and the cluster of gas and stars which **is** bound to it will sink to the bottom of the new galactic potential via dynamical friction (Begelman et al. 1980; Chandrasekhar 1943). Once the separation of the binary is such that its binding energy is greater than that of the surrounding star cluster, the binary is considered hard, meaning that binaries with separation

$$a_h \lesssim 2.8 \text{pc} (1+q)^{-1} (1+1/q)^{-1} \left(\frac{M}{10^8 M_\odot} \right) \left(\frac{\sigma}{200 \text{kms}^{-1}} \right)^{-2} \quad (1.4)$$

can safely be treated as a Keplerian binary (*e.g.* Merritt & Milosavljević 2005). Here σ is the stellar velocity dispersion of the nuclear star cluster and $q \equiv M_2/M_1$, with the individual BH masses satisfying $M_2 \leq M_1$ and $M_1 + M_2 = M$.

Whether the binary becomes hard within a Hubble time depends on the mass ratio of the binary, the amount of gas in the surrounding environment, and the initial orbital parameters of the merger (Mayer 2013). While it is fairly certain that near equal mass galaxy mergers (with nearly equal mass BHs) will quickly form hard MBHBs in less than a galactic dynamical timescale (Mayer et al. 2007; Chapon et al. 2013), the case is not so clear cut for disparate mass ratio mergers. If, for example, the mass ratio of merging BHs and galaxies is 1:10, then it is possible for the tidal disruption time of the smaller BH and its surrounding nuclear star cluster to be shorter than the



dynamical friction migration time. Because the dynamical friction timescale scales inversely with the total mass of the BH and the matter bound to it (Chandrasekhar 1943; Colpi & Dotti 2011), such a scenario could leave the smaller BH alone wandering naked in the galaxy (Callegari et al. 2011; Mayer 2013). This is an example of how observations of MBHBs at close separation, via GWs or the EM signatures discussed in this thesis, and knowledge of their accretion history, will be vital in determining the conditions that do (or do not) create disparate mass ratio binaries in galactic mergers.

Once the MBHB hardens into a Keplerian binary, it must rely on stars which come within $\sim 3a$ of the binary to efficiently remove angular momentum and cause further shrinkage (Saslaw et al. 1974). However, in a closed (not replenished), spherical stellar system there are simply not enough stars on centrophilic orbits to bring the binary to merger within a Hubble time. The reason is that the mass in stars needed to merger the binary is of order a few times the mass of the smaller BH (Merritt & Milosavljević 2005), but such stars undergoing this ‘gravitational slingshot’ mechanism are removed from orbits which can further interact with the binary. Without a way to refill stars into the region of energy-angular momentum space (the loss-cone) that allows nearly radial orbits to interact with the binary, the binary falls at a separation just below a_h .

This situation has been deemed the final parsec problem (FPP Milosavljević & Merritt 2003). A number of ideas have been developed to solve the FPP, including non-spherical stellar distributions which torque stars into the loss cone over time, massive perturbers such as giant molecular clouds, and the migration of the binary through a gaseous disk (Goicovic et al. 2016; Gould & Rix 2000; Armitage & Natarajan 2002). However the FPP is overcome (or not overcome), if the binary separation can shrink to of order $0.05 - 0.15$ pc (for $q = 1 \rightarrow 0.1$), then gravitational radiation will take over and merge the binary within a Hubble time (Peters 1964), generating the loudest sources of gravitational radiation in the universe. This gravitational radiation will be a primary target of the PTAs and eLISA both as individual events and as a stochastic background.

In the work presented here we consider the case where the binary is surrounded by an ample supply of gas in the pc to sub-pc regime. Torquing of gas to the central regions of a galaxy is expected to occur during the galactic merger process (Barnes & Hernquist 1992; Barnes & Hernquist 1996), after which the gas can cool and form into a disc (Barnes 2002). This gas could be important for solving the FPP and altering binary parameters, affecting GW waveforms near merger (*e.g.* Armitage & Natarajan 2005; Yunes et al. 2011; Roedig & Sesana 2012). Interaction with gas is also important for determining the rate of GW events detectable by LISA and the PTAs, as well as the level of stochastic GW background due to MBHBs (Kocsis & Sesana 2011; Shannon et al. 2015; Sesana et al. 2016; Lentati et al. 2015; Arzoumanian et al. 2015). In addition to its importance for orbital dynamics, the gas surrounding a hard MBHB will be vital for creating unique EM signatures of the binary during early inspiral (Part I of this thesis), merger (Chang et al. 2010a; Baruteau et al. 2012; Cerioli et al. 2016) and post merger (Lippai et al. 2008; Corrales et al. 2010; Rossi et al. 2010; Ponce et al. 2012; Rosotti et al. 2012; Zanotti 2012) via accretion and shocks. Understanding these potential EM signatures, requires knowledge of the binary and disk interaction, a rich topic which we now review.



1.1.2 Interaction with a gas disk

The interaction of a gas disk and a binary has been studied extensively in the astrophysical literature as it manifests in a large variety of systems. These include proto-planetary disks (*e.g.* Ward 1997), young binary star systems (*e.g.* Artymowicz & Lubow 1994), the rings around planets (Goldreich & Tremaine 1978), and AGN scale disks surrounding MBHBs (*e.g.* Gould & Rix 2000). Though the physics describing tidal coupling between gas and binary is the same in each case, the specifics of scale can differ in an important way. An example directly relevant to the work in Part I of this thesis, is the mass ratio of the binary. In the case of planets and planetary rings, the secondary body (the smaller mass planet, or the moon in a planetary ring) is much smaller than the primary body

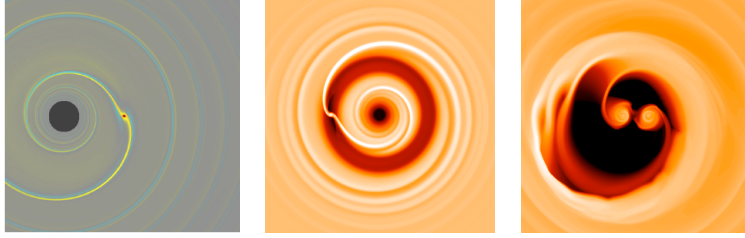


Figure 1.1: The left panel is for a binary with $q \equiv M_2/M_1 = 10^{-6}$ (adapted from (Duffell & MacFadyen 2012)), such a small secondary excites linear spiral density waves in the disk causing Type I inward migration of the binary. The middle panel is for a binary with $q = 10^{-3}$. The dark ring in the orbit of the smaller black hole is the low density gap synonymous with Type II migration. The right panel depicts the clearing of a central (time-fluctuating), low density cavity around an equal mass binary.

(the star or, the ringed planet) because it formed from the leftovers of the primary. In the case of our solar system, the planets grew out of a protoplanetary disk with total mass much less than that of the Sun; the Sun-Earth mass ratio is $\sim 10^{-6}$ while the Sun-Jupiter mass ratio is 10^{-3} . Binary star systems and MBHB systems, however, have the propensity to form with mass ratios closer to unity (for MBHBs see previous section, for stars see Curé et al. 2015)). This variation in typical mass ratio across systems results in drastically different expected behavior of the binary and disk in each system. Here we introduce the typical regimes as they vary with binary mass ratio.

Lin & Papaloizou (1979b,a), Goldreich & Tremaine (1979), and Goldreich & Tremaine (1980) laid the groundwork for disk interactions with very small mass ratio systems, where the response of the binary and disk can be explored with linear perturbation analysis. In this case, the secondary launches linear spiral density waves from the locations of Linblad resonances in the disk (Lynden-Bell & Kalnajs 1972). Summing contributions from torques exerted on the disk at these resonances, Goldreich & Tremaine (1980) were the first to show that the back-reaction of the disk perturbations onto the binary cause the binary orbital separation to change. For disks with Keplerian rotation profiles, inward torques on the secondary from the outer Linblad resonances outweigh the outward torques on the secondary from the inner Linblad resonances, and inward ‘migration’ (orbital

shrinkage) occurs [Ward \(1986\)](#). This process, where linear spiral density waves are launched by the secondary and cause the binary's orbit to shrink, is called Type I migration (See also [Meyer-Vernet & Sicardy 1987](#); [Ward 1997](#); [Tanaka et al. 2002](#); [Tanaka & Ward 2004](#)). Hence, the solutions to the equations of hydrodynamics, for disks perturbed by a small mass ratio binary, consist of wave solutions launched from the position of the secondary. In the frame of the binary, these waves have a stationary phase and once they propagate into the disk on both sides of the binary, the disk approaches a static solution which follows the secondary component as it slowly changes its orbital radius and possibly eccentricity ([Goldreich & Tremaine 1980](#); [Ward 1988](#); [Goldreich & Sari 2003](#)). This steady spiral density wave solution is depicted in the left panel of Figure 1.1.


When the binary mass ratio is large enough, the spiral density waves launched in the disk become non-linear at a short distance (less than a disk scale height) from the secondary ([Goodman & Rafikov 2001](#)). The waves steepen into a shock and deposit angular momentum to the disk material in the co-orbital region of the secondary (see Chapter 3 and also [Dong et al. 2011b,a](#); [Papaloizou & Lin 1984](#); [Lin & Papaloizou 1986](#); [Lin & Papaloizou 1986](#)). This process clears a low density annulus in the orbit of the secondary and is depicted in the middle panel of Figure 1.1. [Lin & Papaloizou \(1986\)](#) argued that if such a gap is formed, the secondary will be locked into the radial flow of the disc, migrating at the viscous inflow rate. Such migration, when a gas barrier is formed around the binary is called Type II migration (see also [Ward 1997](#); [Kley & Nelson 2012](#), and Chapter 3)

Besides the mass ratio, an important difference between different binary+disk systems is the total gas reservoir. Analytical work by ([Syer & Clarke 1995](#); [Ivanov et al. 1999](#)), in one dimension,^d showed that in the non-planetary case, the Type II rate would eventually slow on scales where the mass of the disc becomes smaller than the mass of the migrating binary component. The argument being that the gas no longer has a large enough angular momentum reservoir to shrink the binary

^daveraging disk height and azimuth



separation on the viscous timescale. Hence, this ‘secondary dominated migration’ would cause a pileup of gas behind the secondary and the gas interior to the secondary’s orbit would drain onto the primary creating a central cavity devoid of gas and possibly halting accretion onto the binary. Other 1D arguments (Milosavljević & Phinney 2005) and even early 2D smoothed particle hydrodynamics (SPH) simulations (Artymowicz et al. 1991) concluded that the outward torques from the binary would clear a cavity around most binary systems in the Type II regime.

This picture, while laying the groundwork, has been greatly altered by work in the intervening two decades, notably by the advent of two-dimensional numerical, hydrodynamical simulations which capture the full non-axisymmetric nature of the binary disk interaction, and allow global, time-dependent solutions. The first of such numerical calculations was carried out in Artymowicz & Lubow (1994) and Artymowicz & Lubow (1996) who ran SPH simulations to test analytic work that predicted the sizes of circumstellar disks in binaries and the sizes of the central cavities surrounding the stellar binaries. These SPH simulations showed that particles, in the form of streams tidally ripped from the edge of the cavity wall, could indeed flow past the binary tidal barrier and reach the binary components. The ability of gas to flow past the tidal barrier is of two-fold importance. First, it can allow high levels of accretion onto the binary, which could erate a bright EM signature of the binary, and second, it affects migration (and hence merger) rates of binaries in gas disks. The implications of both are currently areas of active research.

This above 1D studies also naturally fail to account for mass flow across the gap along horse-shoe orbits in the full dimensionality of the problem. Recent work, using 2D viscous hydrodynamical simulations has shown that mass flow across the gap, can allow the secondary to migrate at a rate dependent on disk parameters (density, temperature, pressure), and limited by a maximum migration velocity which can be greater than the viscous rate (Edgar 2008; Duffell et al. 2014; Dürmann & Kley 2015). The mechanisms which dictate the migration rate of gap opening planets in the full two and three dimensional pictures is a topic of ongoing work.

Additionally, chapters 2 (D’Orazio et al. 2013) and 3 (D’Orazio et al. 2016) show that the Type I to Type II regimes are not the only that depend on mass ratio. For binary mass ratios above $q \sim 0.04$, a mass ratio well into the Type II regime for thin disks, the clearing of an annulus in the orbit of the secondary gives way to a much more violent clearing of a lopsided, *central cavity* and time dependent behavior (see the right panel of Figure 1.1). From mass ratios $q \gtrsim 0.3$ the lopsided central cavity is highlighted by an orbiting overdensity at its inner wall. Chapters 2 and 3 provide more details on these transitions and their importance for observing MBHBs.

The work in this thesis focuses on the implications for accretion onto the binary. Hence we now summarize the recent work on this front.

Hayasaki et al. (2007) conducted the first 3D-SPH simulations that specifically targeted MBHB systems with the intent to measure accretion rates onto the binary. Hayasaki et al. (2007) ran simulations of binaries with mass ratios $q = 1.0$ and $q = 0.5$ and binary eccentricities $e = 0.0$ and $e = 0.5$ for up to 60 binary orbits. They find that streams are indeed pulled into a central, low density cavity forming a triple disk system (Hayasaki et al. 2008) consisting of the circumbinary disk and mini-disks around each binary component. The streams promote accretion onto the BHs at rates as high as a tenth of the Eddington rate. For eccentric binaries only, Hayasaki et al. (2007) found a strong modulation in the accretion rate at the binary orbital period.

The SPH simulations of Hayasaki were soon succeeded by the 2D, grid based, **adaptive mesh refinement simulations** of (MacFadyen & Milosavljević 2008, hereafter MM08), run for 1000’s of binary orbits (greater than a viscous time at the position of the binary). These higher resolution simulations, using the FLASH code (Fryxell et al. 2000), are more adept at capturing supersonic dynamics in the vicinity of the binary (shocks). Though MM08 cut out the inner region of the domain containing the binary, they measure accretion rates into the inner boundary which is inside the low density central cavity set by the initial conditions. The high resolution simulation of MM08, for an equal mass binary, found new behavior: the elongation of the central cavity which



results in high levels of accretion into the inner simulation boundary. The resulting periodogram of the accretion rate has the strongest peaks at a low frequency corresponding to $4.5\times$ the binary orbital period and at a frequency corresponding to twice the binary orbital period. Though not discussed in MM08, the cause of accretion variability at these timescales is elucidated in Chapter 2 of this thesis and also [Shi et al. \(2012\)](#) below.

Further SPH studies of MBHB systems were conducted by [Cuadra et al. \(2009\)](#) who ran 3D simulations at a resolution $10 \rightarrow 100$ times higher than that of [Hayasaki et al. \(2007\)](#) for marginally self-gravitating discs with a binary mass ratio of $q = 0.3$ and a simple cooling prescription for the gas. They do not find elongation of the cavity as in MM08, though this could be due to the short amount of time for which the simulations are run, ~ 200 orbits, or the resolution loss that SPH simulations suffer in low density regions (namely the dynamically important cavity edge of the circumbinary disk). [Cuadra et al. \(2009\)](#) do find an accretion rate variable at the orbital period and a propensity for the gas disk to excite binary eccentricity. [Cuadra et al. \(2009\)](#) also finds that the secondary BH has a larger ($\times 2$) accretion rate than the primary due to its closer proximity to the edge of the central cavity.

[Roedig et al. \(2012\)](#) carry out similar simulations to [Cuadra et al. \(2009\)](#), except they start the binary at different initial eccentricities e_0 finding that eccentricity damps for $e_0 \gtrsim 0.6$ but is excited for $e_0 \lesssim 0.6$, suggesting the existence of a rather large preferred binary eccentricity. [Roedig et al. \(2011\)](#) consider different disk thermodynamics and different accretion (sink) prescriptions. In both cases the accretion rates onto these eccentric binaries are found to have periodicity at the binary period and its harmonics, but also at lower frequency disk periods and beat frequencies between disk and binary periods.

The first magneto-hydrodynamical (MHD) simulations of the circumbinary disk were carried out by [Shi et al. \(2012\)](#) with a grid based code. [Shi et al. \(2012\)](#) performed both 2D hydrodynamical and 3D MHD simulations of an equal mass binary on a circular orbit with a similar setup to MM08.

Despite a higher overall accretion rate due to larger viscous stresses generated by the Magneto-rotational instability (MRI), [Shi et al. \(2012\)](#) find similar results to MM08, in that they also find the growth of a lopsided central cavity (elongated with a cavity wall overdensity), which generates variable accretion into the central simulation domain. The variability of the accretion rate is in agreement with MM08, exhibiting a long period variation at the period of gas orbits at the cavity wall, and a second period at twice the binary orbital period (due to the symmetry of an equal mass binary sweeping through the near side of the lopsided cavity). [Shi et al. \(2012\)](#) provide evidence that the cavity lopsidedness is due to the kinematics of stream impacts and recycling of the cavity wall overdensity: the cavity wall overdensity periodically shears apart, causing a lump to orbit around the cavity, feeding streams which are flung out of the cavity again to generate the cavity wall overdensity. [Shi & Krolik \(2015\)](#) have extended upon the above work by considering a range of binary mass ratios, finding qualitative agreement with [D’Orazio et al. \(2013\)](#) and [Farris et al. \(2014\)](#) discussed below.



MHD simulations by [Noble et al. \(2012\)](#) incorporate post-Newtonian corrections to the disk hydrodynamics and binary orbital decay in order to track the disk response through binary inspiral. [Noble et al. \(2012\)](#) find that gas can follow the binary down to separations of $\sim 10M$ with only a $\sim 10 \rightarrow 20\%$ reduction in accretion rate. They also find a lopsided central circumbinary disk cavity, in agreement with MM08, [Shi et al. \(2012\)](#), and the works that we discuss next.

Chapter 2 of this work ([D’Orazio et al. 2013](#)), extends the work of MM08 (using the same numerical code and a similar numerical setup) by considering not only equal mass binaries but a range of binary mass ratios from $q = 0.01 \rightarrow 1$. For an equal mass binary, the qualitative results of disk response and accretion rate variability found in MM08 and ([Shi et al. 2012](#)) are reproduced and compared to the magnitude of accretion for a point mass. By varying q , however, a landscape of accretion variability and magnitude is uncovered and discussion of its use for MBHB searches is discussed.

Farris et al. (2014) extended the work of D’Orazio et al. (2013) by adapting the moving mesh code DISCO (Duffell & MacFadyen 2011; Duffell 2016) to track, for the first time, gas dynamics in the vicinity of the binary using a grid based (rather than an SPH) code. Farris et al. (2014) finds results in agreement with MM08 and D’Orazio et al. (2013) and finds also that the relative accretion rate onto each black hole is a function of mass ratio, dominated by the secondary from $0.05 \leq q < 1$.

For the equal mass case Farris et al. (2015a) considered the effects of gravitational wave decay on the circumbinary disk system showing that gas could indeed follow the binary to small separations causing variable accretion up until merger, contrary to previous lore that gas should be left behind in a ‘decoupling phase’ by a binary that is quickly merging due to GW emission (see 4 for further context).^e Finally Farris et al. (2015b) implemented a simple cooling prescription in DISCO (previous work being for isothermal disks) showing that the variability of the accretion luminosity should indeed follow what was predicted in previous works for the variability of the accretion rate. These results have been key to applying accretion rate variability predictions to the search for close MBHBs discussed in the next section.


Recent work has examined the nature of gas temperature on accretion rates. Both Young & Clarke (2015) and Ragusa et al. (2016) use SPH codes (2D and 3D respectively) to simulate a range of binary mass ratios above $q = 0.1$ and vary the gas temperature. In these simulations, the gas temperature manifests in the form of the disk vertical height to radius aspect ratio, h/r which, in vertical hydrostatic equilibrium, is equal to the ratio of the sound speed to the gas angular orbital frequency at distance r from the system barycenter. A thicker disk, is hotter and has larger pressure forces. Both studies find that, while simulations of accretion onto MBHBs (using $h/r \sim 0.1$) accrete at near the value for a single BH, more realistic, colder AGN discs ($h/r \sim 0.01$) should accrete at much lower rates. Though interesting, the robustness of these results remains to be seen

^ethough this result may be dependent on disk parameters

as numerical difficulties arise in cold disks.

Notably, the simulations of [Ragusa et al. \(2016\)](#) capture the lopsided disk behavior with a circular binary. Except for a study which considered an eccentric binary ([Dunhill et al. 2015](#)), no SPH simulations have captured the lopsided disk behavior. It is not yet clear however what has allowed this change. The SPH works to date are computed with different numerical codes, at different resolutions, and for different total numbers of binary orbits.

The first application of an arbitrary shaped moving mesh code ([Springel 2011](#)) was recently applied to the problem of binary+disk interaction for circular and eccentric stellar binaries by [Muñoz & Lai \(2016\)](#). This work simulates an equal mass binary and finds lopsided cavities and accretion rate variability at the long term period associated with an orbiting cavity wall overdensity and also variability at twice the orbital frequency, in agreement with [D’Orazio et al. \(2013\)](#), [Farris et al. \(2014\)](#), [Shi et al. \(2012\)](#), and [Shi & Krolik \(2015\)](#). For eccentric binaries, [Muñoz & Lai \(2016\)](#) find that the the long-term period is overwhelmed by orbital timescale periodicity and that even for an equal mass binary, one component will accrete more than the other on timescales set by the precession of the lopsided circumbinary disk (see also [Dunhill et al. 2015](#)). Implications of the existence of the long timescale periodicity are discussed in [Chapter ??](#).

In addition to prograde disks in the plane of the binary, some groups have considered retrograde disks ([Nixon et al. 2011a](#); [Roedig & Sesana 2014](#); [Dunhill et al. 2014](#); [Bankert et al. 2015](#); [Nixon & Lubow 2015](#); [Amaro-Seoane et al. 2016](#)) and the [alignemnt](#) or tearing of warped disks ([Nixon et al. 2011b](#); [Nixon 2012](#); [Hayasaki et al. 2013](#); [Nixon et al. 2013](#); [Doğan et al. 2015](#)). 

Also MHD simulations in full general relativity have been carried out by [Farris et al. \(2010, 2011, 2012\)](#); [Gold et al. \(2014b,a\)](#) in the regime just before merger, showing also that accretion rates can be of order the rate expected onto a single BH, periodic, and the gas can follow the binary down to separations of order a few M , allowing the binary to be bright up until merger.

1.1.3 Observations of MBHBs

A motivation for the above theoretical calculations is to determine the types of EM signatures that will identify MBHBs in the inspiral regime. Searching for MBHBs by searching for periodically varying AGN has been proposed before by MM08, [Haiman et al. \(2009\)](#), and by HKM09.^f

HKM09 propose that close MBHBs can be identified in Quasars by their production of EM emission modulated at the binary orbital period. Under this assumption they compute the duty cycle of MBHBs with periods observable in human lifetimes by computing the residence times of MBHBs at a given orbital period (binary separation) taking into account gas induced migration and also GW driven inspiral. Comparison of the residence time to the average Quasar lifetime allows HKM09 to predict the **size** of an EM time domain survey required to capture a specified number of MBHBs at a given orbital period and luminosity.

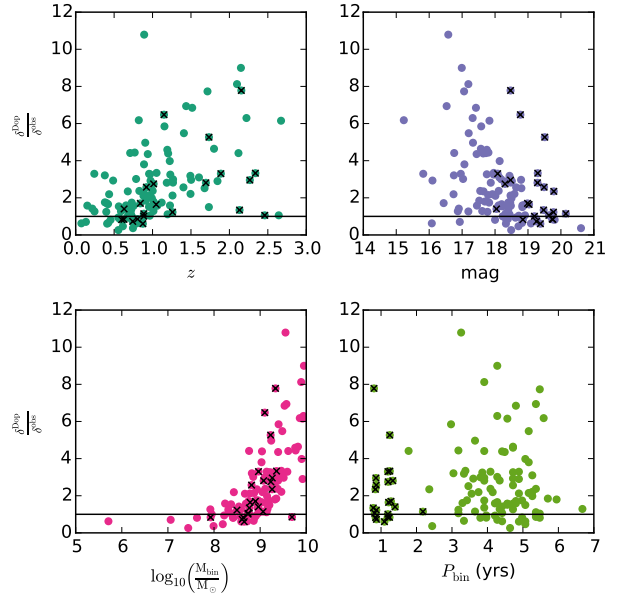


Figure 1.2: A subset of the MBHB candidates from ([Graham et al. 2015b](#)) and ([Charisi et al. 2016](#), denoted by black x's) for which spectral slopes are measured and the magnitude of variability from Doppler boosting can be estimated. From left to right, top to bottom, the ratio of predicted Doppler variability amplitude to observed variability amplitude is plotted vs. redshift, average optical magnitude, log binary mass, and observed period. Candidates above the horizontal black line are possible Doppler boost MBHB candidates.

^fA number of other methods for identifying MBHBs with EM signatures exist in the literature, *e.g.*, spectroscopic signatures of a circumbinary accretion disk, peculiar radio morphology, and broad emission line shifts. For a description of MBHB candidates found through these complimentary methods, see the introduction of [Charisi et al. \(2016\)](#).



Such searches capable of finding EM variability of MBHBs **came to fruition only a year ago** when a group from Caltech/JPL scoured 9 years of time domain optical photometry of $\sim 250,000$ quasars in the Catalina Real-Time Transient Survey (CRTS [Drake et al. 2009](#); [Djorgovski et al. 2010](#); [Mahabal et al. 2011](#); [Djorgovski et al. 2011](#)) attempting to characterize quasar variability. They found a subset of periodically varying sources. The brightest of these sources is PG 1302-102 which was identified as a close, $a \sim 0.01\text{pc}$ separation MBHB candidate by its nearly sinusoidal variability in the V-band continuum. PG 1302 is the first MBHB identified in this manner,^g and **has** the closest reported binary separation at the time of publication ([Graham et al. 2015a](#)). The second part of Part I of this thesis uses the theoretical developments of the first part to interpret the binary candidate PG 1302, finding that PG 1302 is most likely described by a system with a disparate mass ratio where the smaller BH is emitting most of the optical light and modulating it via relativistic Doppler boosting.



Soon after the announcement of PG 1302, 110 more MBHB candidates, were picked out of the CRTS for their periodic optical light curves ([Graham et al. 2015b](#)) and then 33 more, at shorter periods ([Charisi et al. 2016](#)), from the Palomar Transient Factory (PTF [Rau et al. 2009](#); [Law et al. 2009](#)). Figure 1.2 displays a subset of candidates for which Maria Charisi and I have measured the expected maximum amplitude of optical variability due to Doppler Boosting. Comparing to the observed amplitude of variability, Figure 1.2 plots the sample versus various population characteristics and delineates the fraction of the sample which could be caused by the Doppler boost model (see Chapter 5). It is interesting to note that $\sim 80\%$ of the candidates **have** large enough maximum orbital velocities^h to **account for their optical variability**. Because smaller mass ratio binaries are preferred for Doppler Boost candidates (Chapter 5), it is also interesting to note that ([Charisi et al. 2016](#)) find the PTF MBHB candidates to be consistent with a population of low ($q \sim 0.01$) mass

^gThough the MBHB candidate OJ 287 is identified by repeating (though not periodic) flares from over a century of data ([Lehto & Valtonen 1996a](#); [Pursimo et al. 2000](#))

^hmaximum refers to an assumption of an edge on binary inclination and $q \rightarrow 0$

ratio binaries. The characterization of this population of MBHB candidates will be very interesting to track in the near future.

In addition to these discoveries, a few single candidates have been announced from time domain periodicity arguments:

[Liu et al. \(2015a\)](#) report the detection of a ~ 541 day periodicity in the g, r, i, and z bands of the PAN-STARRS1 medium deep survey. At redshift $z = 2$, and with a measured total binary mass of $\sim 10^{10} M_{\odot}$, this puts the putative MBHB candidate at a separation of ~ 10 Schwarzschild radii. Though such a find is extremely unlikely given the short residence times at this separation (HKM09), the hypothesis will be testable as the binary period should speed up as GWs bring the binary to coalescence in the next $\sim 7(1 + z)$ years!

[Zheng et al. \(2015\)](#) report a MBHB candidate in SDSS J0159+0105 with a centi-parsec separation at $z = 0.217$. This interesting object was found in the CRTS, but not with a single period, as the [Graham et al. \(2015b\)](#) search was likely most sensitive to, but with periods at a 2:1 ratio (741 and 1500 days), a characteristic of the simulations of ($q \neq 1$) circumbinary accretion presented here and in other works discussed above.

[Li et al. \(2016\)](#) find evidence for a centi-parsec separation MBHB in the center of NGC 5548. They determine a 14 year orbital period from the optical variability in conjunction with reported orbital variations in the $H\beta$ emission line on the same timescale.

Follow up observations are needed to secure the nature of these candidates. Quasars exhibit intrinsic, wavelength dependent variability [Kelly et al. \(2009\); Kozłowski et al. \(2010\)](#) and it must be confirmed whether or not the observed periodicities are random manifestations of this intrinsic variability. As Jules Halpern says: ‘periodicity is the easiest thing to prove in astronomy, you just have to wait’. However, further evidence, across wavelengths can help pin down the mechanisms driving such periodicity, possibly ruling out models, binary and not, for the production of periodic emission in quasars. Work must be done to place MBHBs in their full gassy, dusty environments in



active galactic nuclei. Then we can begin to piece together a multiwavelength portrait of MBHBs and distinguish them amongst the single BH quasars. The final chapter of Part I (Chapter 6) is a beginning to this process. In Chapter 6, we present a model for the infrared variability expected from dust reverberation by MBHBs that exhibit variable emission, through either accretion variability or anisotropic Doppler boosted emission.

1.2 Part II: Stellar Black Hole + Neutron Star Binaries

The merger of NSs and stellar BHs will generate GWs detectable by the Laser Interferometer Gravitational-Wave Observatory (LIGO [LIGO Scientific Collaboration et al. 2015](#)). Binaries with BHs will generate the highest amplitude GW signals *e.g.* Eq. (1.2), but a binary containing a NS has the most potential to produce a bright EM signal, making BHNS systems especially interesting sources of EM+GW emission.

The tidal disruption of a NS by its BH partner could generate a γ -ray burst after merger ([Narayan et al. 1992](#)). However, it is under-appreciated that most BHs should be large enough to swallow their NSs whole, causing the mergers of most BHNS binaries to be dark. Figure 1.3 plots the simplest approximation for the disruption condition,

$$r_T \approx \left(\frac{M_{\text{BH}}}{M_{\text{NS}}} \right)^{1/3} R_{\text{NS}} \geq r_H(S) = M_{\text{BH}} + \sqrt{M_{\text{BH}}^2 + S^2}, \quad (1.5)$$

which requires that the disruption radius r_T be outside of the BH event horizon with dimensionless spin S (using natural units for the BH horizon radius r_H). Figure 1.3 shows that, unless the BH has near maximal spin, BHNS systems with $M_{\text{BH}} \gtrsim 6M_{\odot}$ will swallow the NS whole! Eq. (1.5) is of course a crude approximation which depends on the (unknown) equation of state of the NS. More sophisticated approximations, however, do not find anything drastically different (*e.g.* [Foucart 2012](#)). Furthermore, the predictions for EM signatures of non-disrupting BHNS mergers, will

be necessary for learning about the NS equation of state once coincident GW observations can be made.

Although the distribution of BH masses which will merge with a NS is unknown, it is interesting to note that the BH mass distribution inferred from BHs in X-ray binaries peaks around $8M_{\odot}$ (Özel et al. 2010) and the only known BH binary consisted of BHs with masses $\sim 30M_{\odot}$, which would certainly swallow a NS hole (Abbott et al. 2016b). Though suggestive, it is important to keep in mind that each of these formation channels may be independent, and not applicable to a BHNS system.

As additional motivation, LIGO is the most sensitive at a frequency of ~ 200 Hz, this is the gravitational wave frequency at coalescence for a NS of mass $1.4M_{\odot}$ in a circular orbit with a BH of mass few $\sim 100M_{\odot}$. If such binaries occur in nature, they have the potential to be high signal to noise LIGO detections, and will not disrupt the NS. The above motivates an exploration of EM counterparts to non-disrupting BHNS systems.

A possible pathway for bright EM emission by non-disrupting BHNS mergers is through the electromagnetic interaction of the NS magnetosphere and the BH event horizon. In such an interaction, the BH horizon behaves like a conductor (see Thorne et al. 1986, and Chapter 7), spinning and moving through the magnetic fields of the NS. The generation of EM radiation from similar situations, of a conducting body moving through the magnetic fields of another, has been investigated in application to a number of other astrophysical systems, *e.g.* Jupiter and its moon Io (Goldreich

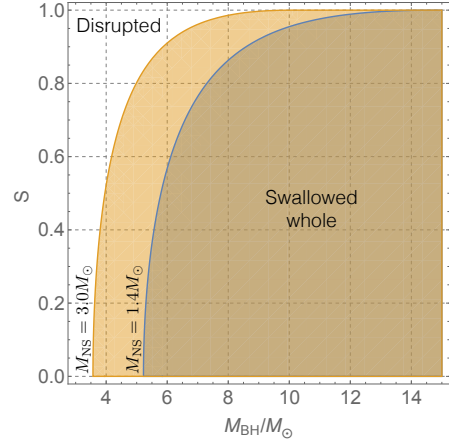


Figure 1.3: Approximate values of black hole mass and spin for which a companion neutron star would be swallowed whole (shaded) vs. disrupted outside of the black hole horizon (unshaded). The two shaded regions are for the labeled neutron star masses, spanning the range of theoretical limits, and for a neutron star with radius 10km.

& Lynden-Bell 1969), planets around white dwarfs (Li et al. 1998) and main sequence stars (Laine et al. 2012; Laine & Lin 2012), binary neutron stars (Vietri 1996; Piro 2012; Lai 2012; Palenzuela et al. 2013), compact white dwarf binaries (Wu et al. 2002; Dall’Osso et al. 2006, 2007; Lai 2012), BHs boosted through magnetic fields (Lyutikov 2011; Penna 2015b), and the Blandford-Znajek (BZ) mechanism (Blandford & Znajek 1977) for a single BH spinning in a magnetic field (for recent numerical work on the BZ mechanism see *e.g.* Palenzuela et al. 2011; Kiuchi et al. 2015).

1.2.1 An analogy from Faraday

To introduce this mechanism, I want to first introduce a similar, though subtle example of the Faraday Disk. The Faraday disk is a type of unipolar inductor constructed by placing a conducting rod through the center of a conducting disk, and running a wire from the top of the rod to the outer edge of the disk, where a sliding contact completes a circuit (see Figure 1.4). Tracing a magnetic field perpendicularly through the disc, and spinning the disk generates an electromotive force (emf), ξ . We can compute the voltage drop from the center of the disk to the edge of the disk from Faraday’s law

$$\xi = -\frac{1}{c} \frac{d}{dt} \int_{\Sigma(t)} \mathbf{B} \cdot d\mathbf{A}, \quad (1.6)$$

where the circuit bounds an open, time-dependent surface $\Sigma(t)$. At first glance, it seems that the emf should be zero, as the obvious loop (loop *a* in Figure 1.4) connecting wire to disk to rod has zero magnetic flux. However, Faraday disks do generate an emf, and this is easily verified by considering the Lorentz force on electrons. To see this from Faraday’s law, recall two restrictions in the choice of the open surface of integration $\Sigma(t)$. One: $\Sigma(t)$ must be bounded by the closed loop through which the emf is computed, and Two: $\Sigma(t)$ must capture the relative motion of the circuit. The key is in the second point: the part of the circuit that starts in the disk must move along

with the spinning disk, otherwise you implicitly assume that the sliding contact and the disk are not in relative motion - but they are by construction.

To calculate the emf, choose loop b in Figure 1.4 which moves along at the rate of the spinning disk, $\Omega = d\phi/dt$. Say that the radius of the disk is R and the uniform magnetic field tracing the disk is \mathbf{B} , then, working in polar coordinates (r, ϕ) ,

$$\xi_{\text{FD}} = -\frac{1}{c} \frac{d}{dt} \int_{\Sigma(t)} \mathbf{B} \cdot d\mathbf{A} = -\frac{1}{c} \int_0^{\phi(t)} \int_0^R B r dr d\phi \quad (1.7)$$

$$= -\frac{1}{c} \int_0^{\phi(t)} \frac{1}{2} \frac{\partial B R^2}{\partial t} d\phi - \frac{1}{c} \frac{B R^2}{2} \frac{d\phi}{dt} = -\frac{B R^2}{2c} \Omega \quad (1.8)$$

where we have used Leibniz's rule of for integration with a time changing limit of integration.

1.2.2 The black hole battery

Remarkably, it turns out that the Faraday disk behaves similarly to a BH moving through a magnetic field. The analogy is spelled out in Part II of this thesis, but if we take for now that the BH orbiting the NS acts as a conductor with size equal to its event horizon (Thorne et al. 1986), then we can calculate the emf generated by the BHNS system.

In the BHNS system, currents are carried by electrons and positrons spiraling along magnetic field lines, hence the sliding wires of the Faraday Disk example are replaced with B-field lines moving across the BH horizon; the same lines of magnetic field generate the magnetic flux piercing the moving BH horizon. Then a closed circuit in the BHNS case traces the B -field lines leaving

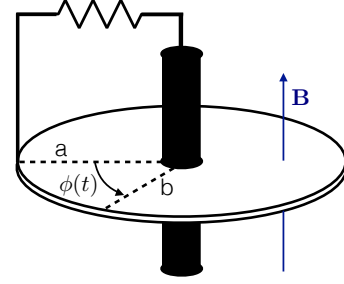


Figure 1.4: Schematic of a Faraday Disk (unipolar inductor).

the NS surface to a time dependent boundary on the BH horizon, crosses the horizon and trace back along a B-field line to the NS. We take the magnetic field to be that of a dipole attached to the NS, $|\mathbf{B}| = B_{\text{NS}} R_{\text{NS}}^3 r^{-3}$, and consider two field lines separated by distance $2R_H$ moving in the x direction relative to the horizon at speed v_f . Then we find a result for the horizon voltage analogous to the Faraday Disk case, and nearly identical to that presented in Chapters 7 and 8,

$$\xi_{\text{BH}} = -\frac{1}{c} \frac{d}{dt} \int_{\Sigma(t)} \mathbf{B} \cdot d\mathbf{A} = -\frac{\pi R_H}{c} \int_0^{v_f t} B(r) dx \quad (1.9)$$

$$= -\frac{\pi R_H}{c} \int_0^{v_f t} \frac{\partial B(a)}{\partial t} dx - \pi R_H B(r) \frac{v_f}{c} \quad (1.10)$$

$$\sim -R_H \left[r \frac{(\Omega_{\text{bin}} - \Omega_{\text{NS}})}{c} + \frac{R_H \Omega_{\text{BH}}}{c} \right] B_{\text{NS}} \left(\frac{R_{\text{NS}}}{r} \right)^3 \quad (1.11)$$

Here we have assumed that $B(r)$ does not vary across the BH horizon and evaluate it at the binary separation $r = a$. In the last line we have written v_f in terms of the binary orbital frequency Ω_{bin} , NS spin frequency Ω_{NS} , and BH horizon spin frequency Ω_{BH} (see [McWilliams & Levin 2011](#)). This becomes the maximum voltage over one hemisphere when R_H is the horizon radius. We call the mechanism which generates this voltage in the BHNS system, the BH-battery.

In the case of the Faraday Disk, the energy which can be harvested electromagnetically (*e.g.*, by heating the resistor in Figure 1.4) comes from the energy put into spinning the disk. In the case of a BHNS binary, the electromagnetic potential energy of the induced horizon voltage comes from the binary orbital energy, and as detailed in Part II of this thesis, the available electromagnetic energy could power luminosities observable from galactic distances (kpc) out to cosmic distances (Gpc) depending on the NS magnetic field strength at merger.

This result, that BHNS binaries could power high luminosity EM counterparts without disrupting the NS was first put forth by [McWilliams & Levin \(2011\)](#). This work was expanded upon by Chapter 7 of this thesis [D’Orazio & Levin \(2013\)](#), which finds relativistic solutions for the EM

fields of a magnetic dipole, in arbitrary motion outside of a horizon.

Numerical works have recently tackled this problem in general relativistic, force-free simulations, which solve the Einstein-Maxwell equations in the limit that $\mathbf{E} \cdot \mathbf{B}$ is everywhere zero, and hence there are no accelerating forces on electrons (Paschalidis et al. 2013). Both types of simulations estimate the observable luminosity via a Poynting flux measured at the outer edge of the simulation domain. The simulation estimates match the analytic arguments of McWilliams & Levin (2011) and D’Orazio & Levin (2013). However, a true understanding of the emission from BHNS systems requires more than this; it requires a radiation mechanism, something to stick into the BH-battery circuit that will shine.

The emission of EM radiation ultimately must come from dissipation of the BH- battery power in the joint BHNS magnetosphere. The classic paper by Goldreich & Julian (1969) shows that if a spinning NS is immersed in its own magnetic dipole field, it generates an electric field with components parallel to the magnetic field. The accelerating \mathbf{E} field rips electrons from the NS crust. The accelerating electrons emit curvature radiation which interacts with the electromagnetic field to generate electron-positrons pairs that go on to generate more curvature radiation and a pair cascade ensues. The pairs move to screen the accelerating electric field, until a force-free condition is met, and the NS is surrounded by the magnetosphere of (Goldreich & Julian 1969). Such a situation halts dissipation of the BH-battery power as long as charges can be replenished to continue screening accelerating electric fields.

However, this does not stop pulsars from shining. As discussed in (Sturrock 1971) and (Ruderman & Sutherland 1975), the force free condition cannot always be sustained globally in the NS magnetosphere. In regions where the force free conditions are violated (*e.g.* $|\mathbf{E}|^2 > |\mathbf{B}|^2$), or where the current density depletes the space charge more quickly than it can be refilled, vacuum gaps must form (*e.g.* Daugherty & Harding 1982; Cheng et al. 1986). In these gaps, a component of the electric field parallel to the magnetic field cannot be totally screened, particles are accelerated,

and dissipation allows the release of EM radiation.

We assume that similar mechanisms are at play in the BHNS example. There need only be gaps in the force free magnetosphere, or magnetic reconnection (though I am not aware of a process by which this will occur in the BHNS magnetosphere) to release the BH-battery power. In Chapter 8 (D’Orazio et al. 2016), we envision such a mechanism, which results in a fireball soon after merger, emitting in the hard X-rays and soft γ -rays. Recently a similar fate has been envisioned for the analogous NSNS system (Metzger & Zivancev 2016). Both of these models may soon be tested by GW observations of coalescing BHNS and NSNS binaries. From such observations we could learn about the NS magnetic field strengths at merger, the NS equation of state, and the dynamics of high energy EM fields in curved spacetime. For now, work can be focused on further understanding dissipation in the BHNS magnetosphere. Stay Tuned.

1.3 Outline of thesis

The rest of this thesis is organized as follows. Chapters 2 through 6 concern MBHBs. Chapter 2 presents hydrodynamical simulations for idealized accretion flows around MBHBs on circular orbits. It is shown that the accretion rates into the cavity cleared by the black holes is traced by accretion streams which can feed the black holes at a rate comparable to that of a single black hole. Furthermore it is shown that, for non-extreme mass ratio binaries, the accretion rates are strongly modulated on timescales which depend on the binary mass ratio. Chapter 3 further explores the transition between strongly modulated accretion flows and steady flows finding dynamical evidence for a transition in CBDs at a binary mass ratio of 1:25. Chapter 3 also explores the dependence of this transition on disk pressure and viscosity. Chapter 4 utilizes the mass ratio dependent theory of accretion rate variability worked out in Chapters 2 and 3 to interpret the MBHB candidate PG 1302-102. Chapter 5 extends this interpretation of PG 1302 in the specific case that

PG 1302 is a binary with mass ratio below the circumbinary disk transition of Chapter 3. In this case, a compelling interpretation for the periodic light curve of PG 1302 is found in the relativistic Doppler Boost model. Chapter 6 places the Doppler boost model in the larger setting of AGN, developing a toy model for the reverberation of optical and UV light by a surrounding dust torus.

Chapters 7 and 8 concern the interaction of NS magnetic fields and a BH horizon. Chapter 7 presents exact relativistic solutions for the vacuum electromagnetic fields of a magnetic-dipole source in arbitrary motion near an event horizon. The solutions are used to interpret and elucidate the electromagnetic circuit which may be hooked up to create high energy EM emission in a BHNS binary. Chapter 8 examines the nature of this high energy EM emission by hooking up a circuit of Chapter 7 to a metaphorical light bulb which manifests in the form of a pair fireball brought on by high energy curvature radiation.